Biophysical Journal
Article

Biophysical Society

Membrane-Bound Alpha Synuclein Clusters Induce Impaired Lipid Diffusion and Increased Lipid Packing

Aditya Iyer,[1,2] Nathalie Schilderink,[2] Mireille M. A. E. Claessens,[2] and Vinod Subramaniam[1,2,3,*]
[1]Nanoscale Biophysics Group, FOM Institute AMOLF, Amsterdam, the Netherlands; [2]Nanobiophysics Group, MESA+ Institute for Nanotechnology, University of Twente, Enschede, the Netherlands; and [3]Vrije Universiteit Amsterdam, Amsterdam, the Netherlands

ABSTRACT The aggregation of membrane-bound α-synuclein (αS) into oligomers and/or amyloid fibrils has been suggested to cause membrane damage in in vitro model phospholipid membrane systems and in vivo. In this study, we investigate how αS interactions that precede the formation of well-defined aggregates influence physical membrane properties. Using three truncated variants of αS with different aggregation propensities and comparable phospholipid membrane binding affinities we show, using fluorescence recovery after photobleaching (FRAP) and fluorescence anisotropy measurements, that formation of αS clusters on supported lipid bilayers (SLBs) impairs lateral lipid diffusion and increases lipid packing beneath the αS clusters. Formation of protein clusters starts immediately after monomer addition. The magnitudes of the changes in effective lipid diffusion and lipid order increase with the protein cluster size. Our results show that the combination of inter-αS and αS-membrane interactions can drive the formation of more ordered lipid domains. Considering the functional involvement of membrane micro-domains in biological membranes, αS-induced domain formation may be relevant for alternative disease mechanisms.

INTRODUCTION

α-synuclein (αS) is a 140 amino acid, intrinsically disordered monomeric protein with a yet unclear physiological function. αS consists of three domains: 1) an N-terminal domain (residues 1–60) with positively charged lysine residues that is believed to be instrumental in membrane binding of monomeric αS (1–4); 2) a central hydrophobic domain known as non-Abeta component (NAC) comprising residues 61–95, which is critical to aggregation of monomers into fibrils and forms the core of the amyloid fibril; and 3) a C-terminal domain (residues 96–140) that is proline rich and predominantly negatively charged at physiological pH (5).

αS is ubiquitously present in eukaryotic cells but is found in particularly high concentrations at the synaptic junctions of neuronal cells (6). Although the function of αS is unclear, it has been suggested to be involved in the regulation of synaptic vesicle pools (7), vesicle trafficking (8,9), and vesicle fusion events at the synapse (10). The mechanism by which αS regulates these processes may depend on physical membrane properties related to domain formation. However, the association of αS with more ordered lipid domains seems to be in conflict with in vitro observations indicating selective binding of αS to liquid disordered regions in anionic lipid membranes (11,12). This discrepancy between in vivo and in vitro observations remains unsolved.

Recent literature indicates that the function of αS is related to changes in the physical properties of lipid membranes upon interaction with monomeric αS (13–16). The macroscopic fluidity of lipid membranes is one such property and is related to the diffusion coefficient of individual lipid molecules and is affected by the packing order of the lipid constituents (17). Fluidity in plasma membranes and membranes of cellular organelles is critical to a multitude of processes in living cells (17) including gene expression (18,19), activity of membrane-bound proteins such as receptor-associated protein kinases (20), sensor proteins (21), ion channels (22), and modulation of immune responses (23). A decrease in membrane fluidity has been predicted to interfere with vesicle fusion and budding (24) and to influence the progression of neurodegenerative diseases including Parkinson's disease (PD) (25,26). Although a lot is known about the aggregation of αS into amyloid structures in PD

Submitted February 10, 2016, and accepted for publication October 13, 2016.

*Correspondence: v.subramaniam@vu.nl

Aditya Iyer's present address is Membrane Enzymology Group, Groningen Institute of Biomolecular Sciences & Biotechnology, University of Groningen, Groningen, the Netherlands.

Editor: Simon Scheuring.

http://dx.doi.org/10.1016/j.bpj.2016.10.016

(27,28), it remains unclear how the intriguing interplay between lipid membranes and αS leads to neuronal cell death in PD (29–34). Considering the functional relevance of αS-membrane interactions in PD, we address in this study how physical membrane properties like membrane packing and fluidity are affected by αS before αS amyloids are observed. Previously, we have shown that after 18 h of incubation of αS, membrane-bound αS amyloids are formed (judged from Thioflavin T positive aggregates) that result in lipid extraction and cause the formation of supported lipid bilayer (SLB) defects (35). Here, we investigate the events preceding amyloid related membrane damage in SLBs. The early changes in physical membrane properties observed here, combined with our previously reported observation on membrane damage at longer timescales, allows us to introduce a sequence of mechanisms by which concentration of membrane-bound αS and aggregation possibly affect lipid membranes.

Using three truncated variants of αS (Fig. 1) with comparable membrane-binding affinities but different aggregation propensities, we probed how lipid order, determined from fluorescence anisotropy experiments, and effective lateral lipid diffusion (D_{LL}), determined in fluorescence recovery after photobleaching (FRAP) experiments, in SLBs were affected by the appearance of surface-bound αS clusters. The Δ71-82-αS (lacking residues 71–82) construct is a known aggregation-deficient variant (36) and has higher net negative charge at pH 7.4 compared with WT-αS. In contrast, 1-108-αS (lacking residues 109–140) is known to aggregate into amyloids much faster than WT-αS (37). The aggregation of the 1-60-αS variant (lacking residues 61–140) has not been investigated in detail yet but this αS variant remained aggregation deficient in our experimental conditions. Both 1-108-αS and 1-60-αS variants have fewer negatively charged residues as compared with WT-αS. The differences in the net charges of the truncated variants gave us a handle to modulate the attractive and repulsive forces between αS monomers.

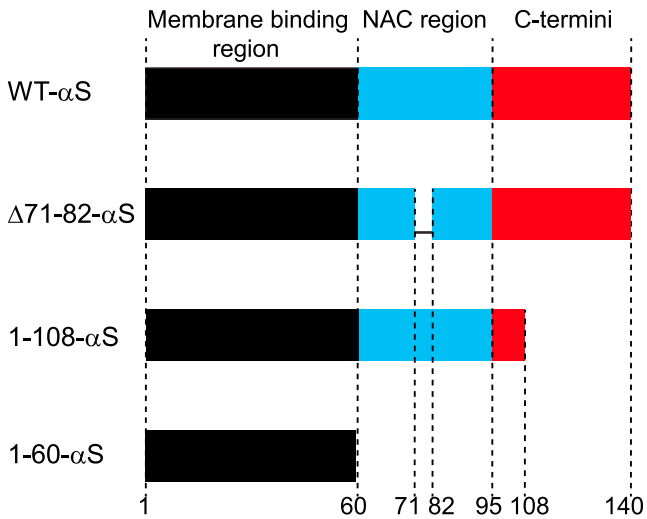

FIGURE 1 Schematic of sequences of WT-αS and the three αS truncated variants used. The truncated variants lacked a significant fraction of the C terminus (1-108-αS), a significant fraction of the NAC region (Δ71-82-αS), or lacked both NAC and C-terminal regions (1-60-αS). To see this figure in color, go online.

Our results show that monomeric αS immediately starts clustering upon addition to SLBs. In these early clusters, no Thioflavin-T-detectable cross-β sheet protein aggregates are present. The size of the early clusters depends on αS concentration and their formation severely impairs the effective D_{LL} in SLBs depending on the αS cluster size. The observed changes in membrane fluidity coincide with an increased lipid order, measured on vesicles using DPH (1,6-Diphenyl-1,3,5-hexatriene) anisotropy and in supported lipid bilayers by microscopic visualization of enhanced DPH fluorescence, upon cluster formation at high protein/lipid (P/L) ratios. Our results indicate that the clustering of αS on lipid membranes induces ordering of underlying lipids.

MATERIALS AND METHODS

Reagents

Stock solutions of 1-palmitoyl-2-oleoyl-sn-glycero-3-phosphocholine (POPC), 1-palmitoyl,2-oleoyl phosphatidylglycerol (POPG), and 1-palmitoyl-2-[6-[(7-nitro-2-1,3-benzoxadiazol-4-yl)amino]hexanoyl]-sn-glycero-3-phosphocholine (NBD-PC) in chloroform were purchased from Avanti Polar Lipids (Alabaster, AL) and used without further purification. Ethylenediaminetetraacetic acid (EDTA) was purchased from Sigma-Aldrich (St. Louis, MO). Sodium chloride (NaCl), sodium hydroxide (NaOH), and 4-(2-hydroxyethyl)-1-piperazineethanessulfonic acid (HEPES) were purchased from Merck (Darmstadt, Germany).

Substrate pretreatment

Before bilayer formation, glass cover-slips were washed in 2% Hellmanex at 80°C for 60 min, rinsed profusely with deionized water, and then dried with a stream of nitrogen gas. The slides were etched for 8 min in a solution of 3:1 (v/v) concentrated sulfuric acid (H_2SO_4) and hydrogen peroxide (H_2O_2). The slides, stored in deionized water throughout, were used within 3 days after treatment.

Supported lipid bilayer preparation

Lipid stock solutions of POPC and POPG in chloroform were mixed in 1:1 molar ratios, dried under a stream of nitrogen gas, and placed under vacuum for 1 h. After drying, the lipid films were rehydrated in 100 mM NaCl solution and mixed in a vortex mixer for 5 min. Small unilamellar vesicles (SUVs) were prepared by sonicating the rehydrated liposome solution for 40 min using a Branson tip sonicator (25% amplitude). Thereafter, the SUVs were centrifuged at 13,200 rpm to remove any tip residue from the sonicator probe. The SUVs were stored at 4°C and used within 3 days. Supported lipid bilayers were formed by vesicle fusion inside a 120 μl custom built chamber on appropriately treated glass slides. The SUVs were mixed with 1 M NaCl solution at a 1:1 ratio to induce fusion. After 20 min incubation, excess vesicles were removed from the chamber by rinsing with 50 mM HEPES, 0.1 mM EDTA (pH 7.4) buffer to remove salt. At least 3 ml of buffer were passed through the chamber to ensure complete solvent exchange. Large unilamellar vesicles (LUVs) for use in aggregation and

fluorescence anisotropy measurements were prepared by rehydrating dried lipid films in 50 mM HEPES, 0.1 mM EDTA (pH 7.4) buffer and extruding 21 times through 100 nm polycarbonate membranes. NBD-labeled lipids in SLBs were imaged using a Nikon (Tokyo, Japan) A1 confocal microscope equipped with a 488 nm laser with a band pass emission filter (525–550 nm), DPH containing SLBs were imaged using a 405 nm laser with a band-pass filter of 450/50 nm. Under the conditions used and based on spectral properties of DPH and AlexaFluor647, Förster resonance energy transfer (FRET) between the two dyes is negligible.

Expression, purification, and labeling of WT-αS variants

All αS variants were expressed in *Escherichia coli* strain BL21(DE3) using the pT7-7 expression plasmid and purified in the presence of 1 mM dithiothreitol (DTT) as previously reported (38). The cDNAs for the truncated variant of αS lacking 71–82 residues (Δ71-82-αS) were obtained from Prof. Benoit Giasson from University of Florida. All αS variants were confirmed to be monomeric using native gel electrophoresis and dynamic light scattering (Fig. S1 in the Supporting Material). Since αS does not contain any cysteine residues necessary for fluorescent labeling, an alanine to cysteine mutation was introduced at residue 140 for WT-αS and Δ71-82-αS. For labeling 1-108-αS and 1-60-αS, a serine to cysteine mutation was introduced at residue 9 (S9C). Earlier NMR studies have confirmed that the S9C mutation in αS does not affect its membrane-bound state (32). S9C has also been used for fluorescence correlation spectroscopy measurements of binding affinities (39). Before labeling, all cysteine containing αS variants were reduced with a sixfold molar excess of DTT for 30 min at room temperature. The samples were desalted with Pierce Zeba desalting columns, followed by the addition of a twofold molar excess of AlexaFluor 647 C2 maleimide dye (Invitrogen, Waltham, MA) and incubated for 2 h in the dark at room temperature. Free label was removed using two desalting steps. The protein labeling efficiency was estimated to be >90% from the absorption spectrum by measuring protein absorbance at 280 nm (A_{280}) using the molar extinction coefficient at 280 nm (i.e., $\varepsilon_{280} = 5120\ cm^{-1}\ M^{-1}$) and including the correction factor for AlexaFluor 647 absorbance ($\varepsilon_{650} = 239{,}000\ cm^{-1}\ M^{-1}$) at 280 nm as 0.03.

Protein cluster imaging and analysis

For imaging of αS clusters, a Nikon A1 total internal reflection fluorescence (TIRF) microscope was used. The labeled proteins were diluted with unlabeled protein (1 in 10) in 50 mM HEPES, 0.1 mM EDTA (pH 7.4) buffer to the desired concentrations before incubating with SLBs. Visualization of SLBs was done by incorporating 0.5 mol% BODIPY-PC in the phospholipid bilayers. The proteins were incubated with the SLBs at room temperature. Images were acquired within 1 min using a 100X oil immersion, 1.49 NA TIRF objective using a 640 nm laser. The acquired images consisted of 512 × 512 pixels with a pixel size of 0.158 μm under identical gain settings. The smallest circular cluster area beyond the resolution limit using Rayleigh's criterion would be 0.14 μm^2. The images were contrast enhanced to the same extent to make any features appear clearly. To quantify the cluster sizes, raw images were first corrected for uneven background illumination (rolling-ball method, 100 pixels) in Fiji (40). The resulting images were subjected to an intensity threshold (consistent for all images) and the resulting pixel areas were quantified as cluster areas.

Fluorescence recovery after photobleaching

To determine the lateral lipid diffusion in SLBs, FRAP was performed on a NikonA1 confocal microscope equipped with a perfect focus system. A 100-mW Argon ion laser (488 nm; Coherent, CA) was used to both bleach and monitor the lipid bilayer fluorescence. In the FRAP experiment fluorescence from a circular region of interest (ROI) was bleached (radius ~8 μm) in 1 s. After bleaching the increase in fluorescence intensity in the ROI was monitored for 6 min. During the experiment there was only a minimal drop in the fluorescence intensity in the reference ROI. All FRAP data were fitted using a Soumpasis fit (41), which has been shown to be a better model for lipid diffusion than a single exponential fit for circular bleach geometries (42).

Circular dichroism spectroscopy

A Jasco (Easton, MD) J-715 spectropolarimeter was used to obtain circular dichroism (CD) spectra at protein concentrations of 3 μM. Spectra were recorded between 215 to 250 nm with a step size of 1 nm and a scanning speed of 10 nm/min, using a 1-mm path length cuvette. The apparent dissociation constants for both the protein variants were determined by titrating them against POPC: POPG (50:50) SUVs and fitting the measured and normalized mean residue ellipticity values at 222 nm to the lipid concentration as reported before (12).

Thioflavin T aggregation assay

Thioflavin T aggregation assays were carried out in a Tecan (Mechelen, Belgium) Infinite M200 micro-plate reader. For every protein variant, 50 μM of monomeric protein was allowed to aggregate in 50 mM HEPES, 0.1 mM EDTA (pH 7.4) buffer at 37°C at 300 rpm in a fluorescence plate reader. The ThT concentration was kept constant at 10 μM. For experiments in presence of liposomes, POPC:POPG (1:1) LUVs were prepared in identical buffer solutions to maintain isotonic conditions and were added in a 1:1 molar ratio to the aggregation mixture.

Fluorescence anisotropy

POPC: POPG (50:50) LUVs with 1 mol% DPH were prepared in 50 mM HEPES, 0.1 mM EDTA (pH 7.4) buffer at room temperature. Lipid concentration was kept constant at 10 μM. Protein concentration was varied to obtain final P/L ratios of 0.02, 0.1, 0.25, 0.5, and 1. Control samples were measured before protein addition in each sample run. Fluorescence anisotropy was recorded at 25°C by using an excitation wavelength of 360 nm and an emission wavelength of 440 nm. The result for each condition is the average of three measurements.

RESULTS

Excess of αS on SLBs promotes protein clustering

To investigate the interplay between αS and lipid membranes, we chose SLBs with an equimolar lipid composition of POPC:POPG. Using this model system, we previously showed that formation of amyloid aggregates of WT-αS on the surface of POPC:POPG SLBs led to membrane disruption and lipid extraction (35). To probe how the clustering of membrane-bound protein that precedes amyloid formation and membrane disruption affects physical membrane properties, we used three different truncated variants (Fig. 1) of αS with varying aggregation propensities. Protein mixtures for each truncated variant and WT-αS containing a fraction of AlexaFluor647-labeled monomers (1 in 10), were added to separate SLBs at varying P/L ratios (0.02 to 1.0) by varying the bulk protein concentration and imaged

within one minute. The addition of protein to the SLB resulted in the immediate appearance of small protein clusters on the SLBs for WT-αS and all truncated variants studied (Fig. 2, *left panel*). Before addition of protein, the SLBs remained defect-free (Fig. S2). On the timescales studied, the clusters were immobile and the clusters did not grow or shrink. Quantification of mean areas of the individual clusters (see Materials and Methods) showed that the area occupied by the individual clusters of WT-αS and the other truncated variants increased with increasing P/L ratio. The size of the Δ71-82-αS clusters seems to saturate around an average protein cluster size of ~0.30 μm^2 from a P/L ratio of 0.25 as shown in Fig. 2 (*right panel*).

At any given P/L ratio, the largest protein cluster sizes were observed for 1-108-αS, followed by 1-60-αS and WT-αS, respectively. The smallest-sized clusters were formed by the Δ71-82-αS variant. Measurement of the area fractions occupied by protein clusters in the fluorescent images showed that the smallest-area fraction was occupied by the Δ71-82-αS variant whereas the 1-60-αS and the 1-108-αS variant occupied the largest-area fractions. Although the area of individual αS clusters increased with increasing P/L ratios, the area fraction occupied by clusters did not vary much (Fig. S2). Because all protein binding sites are already occupied at P/L ratio of 0.02 (12), the addition of more protein beyond this P/L ratio cannot result in formation of new protein clusters. Instead the cluster area increases with increasing P/L ratio with the combined area of all clusters remaining unchanged. This suggests reorganization of the membrane-bound protein clusters into bigger clusters upon increasing P/L ratios. The possibility of three-dimensional growth cannot be completely excluded since the addition of αS to preexisting clusters could be either from the bulk solution or from membrane-bound protein. Although the measured cluster areas are not necessarily equilibrium values, we do not observe any cluster movement or exchange of material between clusters and the bulk solution that is fast enough to result in growth/shrinkage of clusters over the timescale of the experiments. Incubation of monomeric αS with bare glass substrates resulted in homogenous adsorption of the protein and did not result in the formation of protein clusters (Fig. S1). We therefore conclude that the formation of the protein clusters requires the presence of lipid membranes and investigated if it affects the membrane properties.

Clustering of monomeric αS to SLB surface affects lateral lipid diffusion

To explore the changes in physicochemical properties of the membrane due to the presence of αS clusters, we studied changes in membrane fluidity, e.g., lipid diffusion and order. FRAP experiments were performed before (control) and immediately after αS incubation to investigate the influence of αS binding on the effective lateral lipid diffusion coefficient of NBD-PC (henceforth $D_{NBD\text{-}PC}$) in the SLBs. Upon systematically increasing the P/L ratio for monomeric WT-αS and the truncated variants from 0.02 to 1, we observed differences in the drop of the $D_{NBD\text{-}PC}$ (Fig. 3) in the presence of the truncated variants compared with

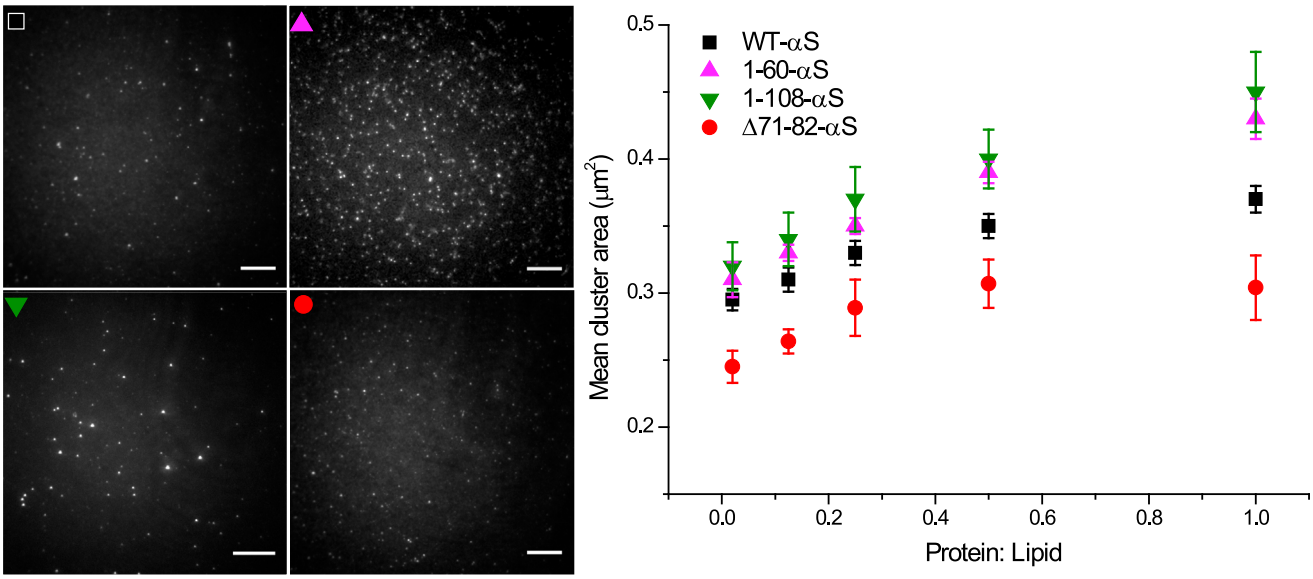

FIGURE 2 Representative fluorescence images of SLBs after addition of monomeric αS. Addition of monomeric αS (10% AlexaFluor 647 labeled) to POPC:POPG SLBs with varying P/L ratios led to immediate formation of clusters. The lipid concentration was calculated (from the dimensions of the flow chamber used and assuming an average lipid headgroup size of 0.65 nm^2) to be 10 μM. Images were acquired immediately after protein incubation (protein channel, *left panel*). The acquired images were subjected to an intensity threshold after background subtraction to estimate the respective mean cluster areas (*right panel*). The error bars are three times the standard error obtained from an average of ~2500 clusters. All experiments were carried out in 50 mM HEPES, 0.1 mM EDTA (pH 7.4) buffer at room temperature. Scale bar is 10 μm. To see this figure in color, go online.

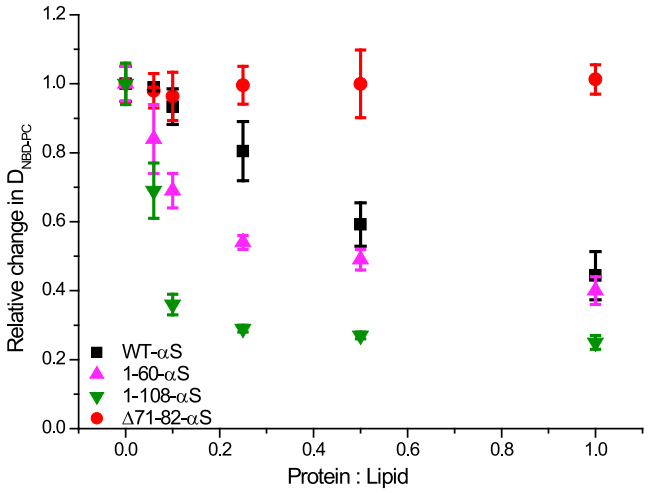

FIGURE 3 αS concentration dependent changes in $D_{NBD\text{-}PC}$ in POPC:POPG (50:50) SLBs. Incubation of increasing concentrations of monomeric αS, or increased P/L ratios consistently resulted in a drop in the $D_{NBD\text{-}PC}$ after protein addition for all αS variants except Δ71-82-αS (*red circles*).The decrease in the $D_{NBD\text{-}PC}$ is more pronounced for the 1-108-αS (*green downward triangles*) and 1-60-αS (*magenta upward triangles*) as compared with WT-αS (*black squares*) for all P/L ratios. The error bars indicate standard deviations obtained from five individual FRAP measurements. All experiments were carried out in 50 mM HEPES buffer, 0.1 mM EDTA (pH 7.4) at room temperature. To see this figure in color, go online.

WT-αS. $D_{NBD\text{-}PC}$ dropped as a function of the P/L ratio by ~55% in the presence of WT-αS at a P/L ratio of 1. At all P/L ratios tested, $D_{NBD\text{-}PC}$ remained unaffected by the presence of the Δ71-82-αS variant even though the binding affinities of WT-αS and Δ71-82-αS are comparable (Fig. S3). The drop in $D_{NBD\text{-}PC}$ was maximal in the presence of the 1-108-αS variant (~75%) followed by the 1-60-αS variant, at all P/L ratios. Interestingly, we did not observe any immobile fraction of NBD-PC upon binding of either truncated variants or WT-αS to the SLBs. Our results are in agreement with previous reports showing impaired lipid diffusion in liposomes upon binding of WT-αS by electron spin resonance spectroscopy (43). Estimation of the number of amino acids involved in the formation of the membrane-bound helical domains of WT-αS and 1-108-αS variant on lipid membranes revealed (Fig. S3) an identical value of ~79 amino acids. The size of the membrane-bound helical domain for the 1-60-αS variant corresponded to ~31 amino acids and ~47 amino acids for the Δ71-82-αS variant. Mere membrane association or the size of the membrane-bound helical domain can thus not explain the trends observed in $D_{NBD\text{-}PC}$ as a function of protein mutations.

The effect of αS binding on membrane fluidity was not only observed for POPC:POPG (1:1) SLBs. FRAP experiments with POPC:POPS (1:1) SLBs showed a similar αS-induced impairment of $D_{NBD\text{-}PC}$, indicating that the effective drop was not specific for the phosphatidylgylcerol (PG) headgroup (Fig. S4). The drop in D_{LL} was also consistently observed for a given concentration of WT-αS, independent of the type of fluorescent lipid used to probe D_{LL} (Fig. S5). Since the selected proteins (Fig. 1) differ in their tendency to aggregate, interactions between membrane-bound proteins that resulted in the formation of membrane-bound protein clusters or amyloid species may be responsible for the observed changes in D_{LL}.

Clusters of αS on lipid bilayers do not contain amyloid signature

To check if the formation of clusters on the membrane surface results in amyloid formation, we monitored the aggregation of WT-αS and the truncated variants in presence and absence of POPC:POPG LUVs using ThT fluorescence. Although ThT-negative amyloid fibrils have been reported for Aβ protein, the increase in ThT fluorescence signal is generally considered indicative of amyloid formation (44,45). As in the FRAP experiments the P/L ratio was varied from 0.02 to 1. The change in ThT fluorescence in time is presented in Fig. 4. In the absence of vesicles, WT-αS had a long aggregation lag-time (~25 h) whereas, the lag-time for 1-108-αS variant was shorter (~3 h). Δ71-82-αS and the 1-60-αS failed to aggregate into amyloids over a period of 10 days. The presence of POPC:POPG liposomes could not enhance aggregation of both Δ71-82-αS and the 1-60-αS at P/L ratios as high as 1.

In the presence of POPC:POPG liposomes, only the WT-αS and the 1-108-αS variant showed an increase in the ThT fluorescence signal. The 1-60-αS (*magenta upward triangles*) and Δ71-82-αS (*red circles*) did not aggregate

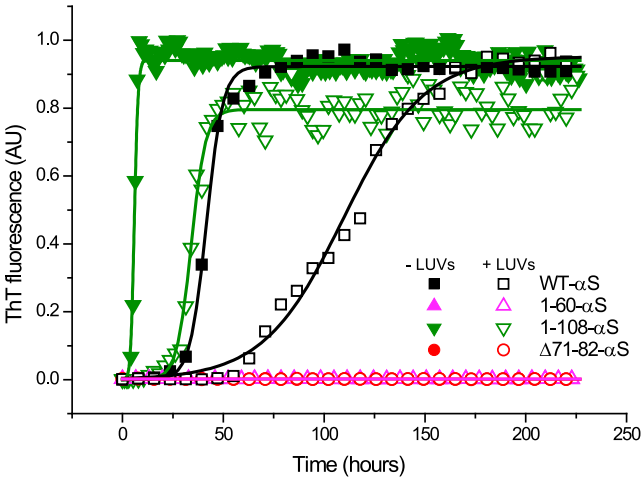

FIGURE 4 Representative aggregation curves of αS truncated variants. The αS truncated variants were aggregated in the presence (*open symbols*) and absence (*solid symbols*) of 1:1 POPC:POPG liposomes. 1-108-αS (*green downward triangles*) aggregated with a lag-time of ~3 h whereas the lag time of the WT-αS (*black squares*) was ~25 h 50 μM of protein of each variant in at least six replicates were allowed to aggregate in 50 mM HEPES, 0.1 mM EDTA (pH 7.4) buffer at 37°C at 300 rpm in a fluorescence plate reader. ThT concentration was kept constant at 10 μM. To see this figure in color, go online.

either in presence/absence of POPC:POPG liposomes over a period of ~10 days. These results are consistent with reports suggesting that the NAC region is required for aggregation of αS. In the presence of POPC:POPG liposomes, we did not observe a ThT fluorescence signal for ~25 h for the 1-108-αS variant and the aggregation lag-time of WT-αS was also significantly extended in the presence of the vesicles. It is therefore unlikely that the drop in D_{LL} observed soon after addition of αS to SLBs results from amyloid formation. Although recent reports have stated that lipid membranes can act as primary nucleation sites and therefore accelerate aggregation of αS into amyloids (46), we did not observe this effect. This discrepancy probably results from the different physical membrane properties of the vesicle model systems used. At room temperature, the POPC:POPG LUV membranes used in our experiments are in a liquid disordered state ($T_{m,}$ −2°C) and have relatively low curvature. The highly curved DMPS SUVs studied in (46) are used below the T_m (35°C) and therefore in a liquid ordered phase. Below T_m considerable stresses can develop in SUVs that promotes the formation of substantial defects to alleviate the strain. Such defects, wherein the hydrophobic core of the membrane is relatively exposed may have a considerable effect on the nucleation of amyloid fibrils. Aggregation competent αS variants showed an increase in the aggregation lag time in the presence of liposomes. The binding of monomers to anionic liposomes may effectively decrease the concentration of αS in solution. This reduction of the αS concentration in the bulk is most likely responsible for the increase in the aggregation lag-time of αS in the presence of liposomes. We also incubated ThT with SLBs in samples with P/L ratio of 1 and observed no fluorescence signal from ThT in the protein clusters within 1 h.

Although accumulation of αS on SLBs resulted in protein clustering at all P/L ratios and lipid compositions for WT-αS and all truncated variants used in the study, conversion of membrane-bound protein to amyloid structures was never observed within experimental times (~60 min). Under identical conditions we have shown previously the formation of amyloid structures after 18 h (35).Therefore, we conclude that the conversion to amyloid structures cannot explain the changes in D_{LL}.

αS binding leads to increased acyl chain packing in lipid membranes

In the absence of membrane-associated amyloid formation, the decrease in the D_{LL} could result from a tighter packing (increased order) of lipids upon cluster formation of αS (47). To test this hypothesis, steady-state fluorescence anisotropy was used to monitor if changes in membrane fluidity resulting from an increase in lipid order in POPC:POPG liposomes. DPH is a well-known hydrophobic probe for structural and dynamic studies on lipid membranes (48). DPH roughly resembles a cylinder with its absorption and fluorescence emission transition dipoles aligned parallel to its long molecular axis. It has negligible fluorescence in solution because of its rotational motion. In absence of rotational motion, it has a very high fluorescence polarization depending on the orientation of the long axis. DPH aligns parallel to the lipid acyl chains and therefore an increase in lipid acyl chain packing can be monitored as an increase in the fluorescence anisotropy, r (49). At a constant DPH concentration, the P/L ratio was varied similar to that in the FRAP measurements. We observed that WT-αS and 1-60-αS showed an increase in anisotropy values with the 1-60-αS showing consistently higher values at all P/L ratios. Despite having a comparable membrane binding affinity as WT-αS, Δ71-82-αS only shows a marginal change in the steady-state anisotropy, r as shown in Fig. 5.

The 1-108-αS variant showed a steep increase at low P/L ratios and continued to increase at higher P/L ratios. The changes in steady-state anisotropy seem to be maximal for the 1-108-αS variant indicating increased packing of lipid acyl chains in the presence of clusters of this protein. To further test if we could visualize the protein-induced ordering of acyl chains in lipid membranes, WT-αS and other truncated variants were added on SLBs containing 1 mol% DPH at a P/L ratio of 1 (Fig. 6). The addition of αS to POPC:POPG SLBs containing 1 mol% DPH result in intensely fluorescent regions beneath all clusters of all αS species except the Δ71-82-αS variant (Fig. 6). Increasing the concentration of WT-αS that was incubated with the DPH-labeled POPC:POPG SLBs resulted in larger WT-αS clusters and corresponding larger regions in which the lipid

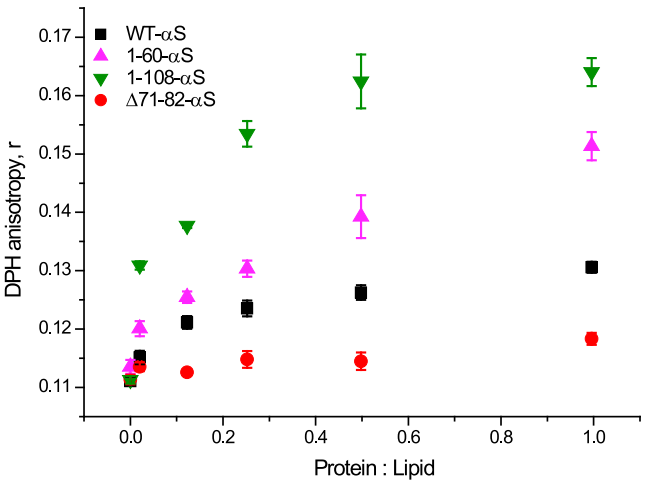

FIGURE 5 Changes in DPH anisotropy in POPC: POPG (1:1) LUVs with increasing αS concentration. Addition of monomeric αS to POPC: POPG LUVs containing 1 mol% DPH leads to a pronounced increase in the fluorescence anisotropy in all truncated variants and WT-αS (*black squares*) except Δ71-82-αS (*red circles*). The 1-108-αS (*green downward triangles*) and 1-60-αS (*magenta upward triangles*) show higher anisotropy values at all P/L ratios compared with WT-αS. The error bars indicate standard deviations obtained from three independent measurements. All experiments were carried out in 50 mM HEPES, 0.1 mM EDTA (pH 7.4) buffer at room temperature. To see this figure in color, go online.

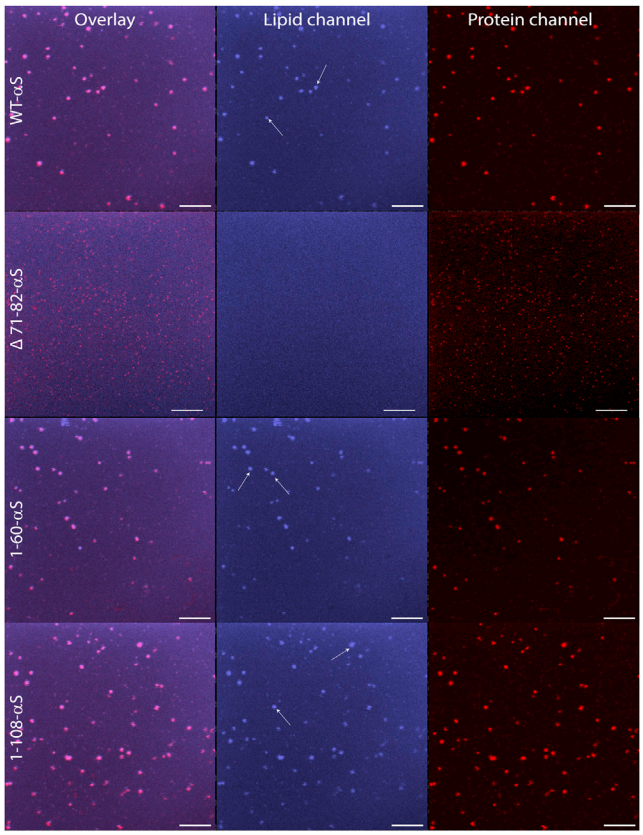

FIGURE 6 Lipid ordering in POPC:POPG SLBs observed using DPH in presence of αS. WT-αS and other truncated variants were added to 1 mol% DPH containing POPC:POPG SLBs at a lipid to protein ratio of 1. Control images (no protein added) do not show any regions with enhanced fluorescence. After addition of αS to SLBs, enhanced fluorescence is observed in the lipid channel below regions of αS clusters (*white arrows in lipid channel*) for all αS constructs except Δ71-82-αS. All experiments were carried out in 50 mM HEPES buffer, 0.1 mM EDTA (pH 7.4) at room temperature. The scale bar is 10 μm. To see this figure in color, go online.

packing was more ordered (Fig. S6). These observations combined with the marginal changes in the steady-state anisotropy of DPH in liposomes in the presence of the Δ71-82-αS variant suggest little or no influence on lipid packing. Results from steady-state anisotropy and the ordered domains that become visible in experiments with DPH-labeled POPC:POPG SLBs thus indicate that lipid packing and cluster formation are linked.

DISCUSSION

In this study, we have systematically investigated how, preceding conversion to amyloid aggregates as shown previously (35), clustering of monomeric αS and the interaction of αS clusters with lipid membranes influence physicochemical properties of lipid membranes. At the conditions of our experiments, all αS binding sites on the membrane surface are occupied, the average distance between two membrane-bound monomers is small and interprotein collisions can result in cluster formation. Clustering of membrane-bound αS is a consequence of a complex interplay mainly between attractive hydrophobic interactions, resulting from the solvent exposed hydrophobic patches on the membrane-bound αS, and repulsive electrostatic interactions, resulting from the negatively charged unstructured solvent exposed C-terminal region of αS. Considering the interplay between attractive and repulsive forces, the net interprotein repulsion is expected to be highest in the Δ71-82-αS and minimal in the 1-108-αS variant. Thus, the Δ71-82-αS results in smaller-sized clusters due to decreased hydrophobic attraction between proteins compared with WT-αS. The removal of the negatively charged C-terminal region in two truncated variants (1-60-αS and 1-108-αS) results in larger clusters than WT-αS that is likely because of decreased electrostatic repulsions between the membrane-bound monomers. It has been reported that αS can induce local curvature in lipid membranes (13). It is possible that the αS binding-induced increase in local membrane curvature enhances binding of additional αS, probably in a cooperative manner. The observed changes in lipid diffusion are not a result of a mere association of αS monomers and the SLBs. This is because, despite having similar membrane-bound fractions as WT-αS, membrane-bound Δ71-82-αS has no influence on D_{LL}. Also, at P/L ratios ~0.02 where the lipid binding sites for αS are completely saturated, we observe no change in D_{LL}. The changes in D_{LL} are thus a consequence of interactions of the αS clusters with lipid membranes.

The mobile fraction of the fluorescent lipid probe (either zwitterionic or negatively charged) remained close to unity at any P/L ratio. This means that the lipids are not immobilized under the protein clusters but are able to exchange continuously. Upon increasing the bulk protein concentration systematically, we observe that that the mean cluster area increases but the total area occupied by these clusters does not change significantly. This suggests that a higher αS concentration in the bulk allows for a faster rearrangement of clusters by exchange with bulk protein. As the cluster area increases, the time a particular lipid spends under a αS cluster (first passage time) increases. Since FRAP measures an *effective* diffusion coefficient of lipids in an area that contains both regions with and without clusters, the D_{LL} obtained in presence of clusters is a weighted average of the diffusion coefficients from both regions, where large clusters have a larger effect on the effective diffusion coefficient than smaller ones. The accumulation of proteins in clusters results in an accumulation of more closely packed (charged) lipids under the clusters as seen from fluorescence microscopy and an increase in lipid order as indicated by steady-state anisotropy. It is known that an increase in lipid order, by increasing cholesterol content or degree of saturation, can significantly decrease D_{LL} (47). For a similar packing of proteins in the clusters one would expect the lipid organization under the clusters to be independent of the

cluster size. Without single lipid tracking measurements, it however is difficult to ascertain if the resulting drop in D_{LL} beneath αS clusters is similar for larger and smaller clusters. However the data points from both the FRAP and DPH anisotropy experiments on SLBs covered with protein clusters of the different truncated variants collapse on a single "master" curve (Fig. 7). The increase in lipid order and the decrease in D_{LL} both become visible beyond a cluster area of ~0.30 μm^2, a value well above the diffraction limited area under our imaging conditions (~0.14 μm^2).

The correlation between the changes in D_{LL} and r suggest a concerted process where the formation of clusters leads to a closer packing of lipids and a decrease of the effective D_{LL}. The correlation between the effective D_{LL} and r as observed in the master curve is nontrivial as it does not result from a direct interaction between proteins and lipids. Although αS mainly binds to anionic lipids, the drop in effective D_{LL} of zwitterionic lipids suggests that αS clustering (possibly stabilized by anionic lipids) also affects effective D_{LL} of zwitterionic lipids. A similar effect on the diffusion of zwitterionic lipids has been observed for annexin a5, a peripheral protein involved in vesicle fusion events, upon its clustering on anionic lipid membranes (50).

The results obtained in this study, supplemented by our previous work on the effect of αS binding at longer timescales (35), now gives us a complete sequence of events by which αS accumulation and aggregation on membranes possibly interfere with membrane function and integrity. Upon binding to model lipid membranes at low P/L ratios, αS clusters are not observed and αS binding-induced changes in physical properties of membranes are insignificant. Upon increasing the P/L ratio or incubation times, the membrane-bound protein reorganizes into ThT-negative micrometer-sized clusters that increase the packing order of the underlying lipids and impair lipid diffusion. Upon attaining amyloid conformation at longer incubation times, αS aggregates cause significant membrane damage by extracting lipids from the bilayer that result in the formation of membrane defects.

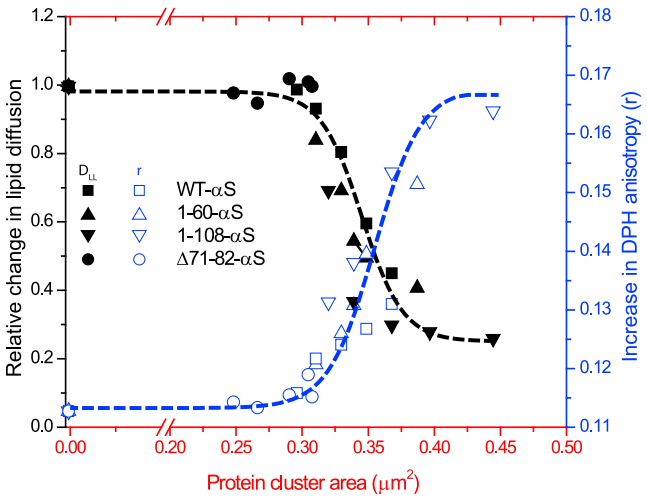

FIGURE 7 Master curve of data correlating changes in lipid diffusion and lipid packing to protein cluster areas. The above plot shows relative changes in the lipid diffusion coefficients (*black solid symbols*) and absolute steady-state anisotropy values of DPH in liposomes (*blue open symbols*) against mean protein cluster areas. WT-αS is depicted as squares whereas the Δ71-82-αS variant is shown as circles. The 1-108-αS variant (*downward triangles*) results in the biggest change in lipid diffusion coefficients and DPH anisotropy followed by the 1-60-αS variant (*upward triangles*). The dotted lines are representative of the general trend in increasing anisotropy (*blue lines*) and changes in lipid diffusion (*black lines*). To see this figure in color, go online.

Previous reports have shown that αS binding to lipid membranes seems to decrease the packing order in lipid mixtures that form liquid-ordered membranes (51). Our results suggest that αS clusters can increase the overall lipid packing order in lipid mixtures that form liquid-disordered membranes. These observations suggest, albeit from in-vitro observations, that αS may play a role in the regulation of lipid packing in cell membranes. Clustering of proteins and ordering of lipids into membrane microdomains are both known to be involved in protein function and this interplay forms the basis for many cellular signaling processes (52). Protein clustering and the formation of membrane domains can either be mutually exclusive or coupled depending on the cellular niche (53–55). Binding studies of αS with synaptic vesicle mimics in vitro suggest a strong preference for membrane curvature, cholesterol content, and lipid phase (12,56,57). The decreased membrane fluidities could also be relevant in the pathogenic aspect of αS. Aging cellular membranes in particular have lower membrane fluidity and their intrinsic membrane recycling mechanisms are less efficient (58). The closure of transient defects in plasma membranes, which would be expected to reseal quickly, would be less efficient with decreased membrane fluidities. Our finding that the clustering of αS causes impaired fluidity and ordering of lipids provides a biophysical perspective in understanding the functional/pathogenic role of αS.

CONCLUSION

Our data suggest that the formation of non-amyloid αS clusters upon exposure of SLBs to αS at high P/L ratios changes both the effective lipid diffusion and lipid packing. The observation that an increase in lipid order and decrease in D_{LL} as a function of the mean area of individual clusters can be plotted on a master curve suggest that the close packing of lipids in the clusters is responsible for the observed effect. Changes in physical properties of membranes due to αS monomers or clusters could be relevant to the function of αS bound to membranes in cellular systems. Subtle changes resulting from increased αS concentrations or mutations might change αS clustering and thereby affect lipid diffusion, partitioning, reorganization, and ordering

that could give undesirable biological consequences and is possibly relevant in PD.

SUPPORTING MATERIAL

Six figures are available at http://www.biophysj.org/biophysj/supplemental/S0006-3495(16)30943-2.

AUTHOR CONTRIBUTIONS

A.I., M.M.A.E.C., and V.S. designed and analyzed the experiments. A.I. performed most of the experiments. N.S. designed and constructed vectors for expression of variant proteins and performed binding experiments using CD spectroscopy with the 1-108-αS variant. A.I., M.M.A.E.C., and V.S. wrote the manuscript. All authors reviewed the results and approved the final version of the manuscript.

ACKNOWLEDGMENTS

We thank Prof. Benoitt Giasson from University of Florida for providing the plasmids for the Δ71-82-αS construct; Prof. Roberta Croce from the Vrije Universiteit Amsterdam for access to instrumentation for CD spectroscopy measurements; Dr. Kapil D. Singh from University of Zürich for providing a script for FRAP data analysis; and Prof. Nils O. Petersen from University of Alberta, Dr. Martin Stöckl from University of Konstanz, and Yuval Mulla from FOM Institute AMOLF for discussions.

The work presented here is part of a project titled "A Single Molecule View on Protein Aggregation" (No. 127) funded by the Foundation for Fundamental Research on Matter (FOM).

SUPPORTING CITATIONS

Reference (59) appears in the Supporting Material.

REFERENCES

1. Zarbiv, Y., D. Simhi-Haham, …, R. Sharon. 2014. Lysine residues at the first and second KTKEGV repeats mediate α-synuclein binding to membrane phospholipids. *Neurobiol. Dis.* 70:90–98.
2. Lorenzen, N., L. Lemminger, …, D. E. Otzen. 2014. The N-terminus of α-synuclein is essential for both monomeric and oligomeric interactions with membranes. *FEBS Lett.* 588:497–502.
3. Jo, E., J. McLaurin, …, P. E. Fraser. 2000. α-synuclein membrane interactions and lipid specificity. *J. Biol. Chem.* 275:34328–34334.
4. Davidson, W. S., A. Jonas, …, J. M. George. 1998. Stabilization of α-synuclein secondary structure upon binding to synthetic membranes. *J. Biol. Chem.* 273:9443–9449.
5. Kim, T. D., S. R. Paik, and C. H. Yang. 2002. Structural and functional implications of C-terminal regions of alpha-synuclein. *Biochemistry.* 41:13782–13790.
6. Nemani, V. M., W. Lu, …, R. H. Edwards. 2010. Increased expression of alpha-synuclein reduces neurotransmitter release by inhibiting synaptic vesicle reclustering after endocytosis. *Neuron.* 65:66–79.
7. Murphy, D. D., S. M. Rueter, …, V. M. Y. Lee. 2000. Synucleins are developmentally expressed, and alpha-synuclein regulates the size of the presynaptic vesicular pool in primary hippocampal neurons. *J. Neurosci.* 20:3214–3220.
8. Vargas, K. J., S. Makani, …, S. S. Chandra. 2014. Synucleins regulate the kinetics of synaptic vesicle endocytosis. *J. Neurosci.* 34:9364–9376.
9. Scott, D., and S. Roy. 2012. α-synuclein inhibits intersynaptic vesicle mobility and maintains recycling-pool homeostasis. *J. Neurosci.* 32:10129–10135.
10. Burré, J., M. Sharma, …, T. C. Südhof. 2010. Alpha-synuclein promotes SNARE-complex assembly in vivo and in vitro. *Science.* 329:1663–1667.
11. Stöckl, M., P. Fischer, …, A. Herrmann. 2008. Alpha-synuclein selectively binds to anionic phospholipids embedded in liquid-disordered domains. *J. Mol. Biol.* 375:1394–1404.
12. Shvadchak, V. V., L. J. Falomir-Lockhart, …, T. M. Jovin. 2011. Specificity and kinetics of alpha-synuclein binding to model membranes determined with fluorescent excited state intramolecular proton transfer (ESIPT) probe. *J. Biol. Chem.* 286:13023–13032.
13. Braun, A. R., E. Sevcsik, …, J. N. Sachs. 2012. α-synuclein induces both positive mean curvature and negative Gaussian curvature in membranes. *J. Am. Chem. Soc.* 134:2613–2620.
14. Ouberai, M. M., J. Wang, …, M. E. Welland. 2013. α-synuclein senses lipid packing defects and induces lateral expansion of lipids leading to membrane remodeling. *J. Biol. Chem.* 288:20883–20895.
15. Hellstrand, E., M. Grey, …, E. Sparr. 2013. Adsorption of α-synuclein to supported lipid bilayers: positioning and role of electrostatics. *ACS Chem. Neurosci.* 4:1339–1351.
16. Ulmer, T. S., A. Bax, …, R. L. Nussbaum. 2005. Structure and dynamics of micelle-bound human alpha-synuclein. *J. Biol. Chem.* 280:9595–9603.
17. Shinitzky, M. 1984. Membrane fluidity in malignancy. Adversative and recuperative. *Biochim. Biophys. Acta.* 738:251–261.
18. Los, D. A., K. S. Mironov, and S. I. Allakhverdiev. 2013. Regulatory role of membrane fluidity in gene expression and physiological functions. *Photosynth. Res.* 116:489–509.
19. Mironov, K. S., E. G. Maksimov, …, D. A. Los. 2012. Feedback between fluidity of membranes and transcription of the desB gene for the omega 3-desaturase in the cyanobacterium *Synechocystis*. *Mol. Biol.* 46:134–141.
20. Hohmann, S. 2002. Osmotic stress signaling and osmoadaptation in yeasts. *Microbiol. Mol. Biol. Rev.* 66:300–372.
21. Tokishita, S., and T. Mizuno. 1994. Transmembrane signal transduction by the *Escherichia coli* osmotic sensor, EnvZ: intermolecular complementation of transmembrane signalling. *Mol. Microbiol.* 13:435–444.
22. Sukharev, S. 1999. Mechanosensitive channels in bacteria as membrane tension reporters. *FASEB J.* 13 (*Suppl.*):S55–S61.
23. Deliconstantinos, G. 1987. Physiological aspects of membrane lipid fluidity in malignancy. *Anticancer Res.* 7 (5B):1011–1021.
24. George, J. M., and M. L. Yang. 2000. α-synuclein physiology and membrane binding. *In* Madame Curie Bioscience Database [Internet]. Landes Bioscience, Austin, TX.
25. Maccarrone, M., G. Bernardi, …, D. Centonze. 2011. Cannabinoid receptor signalling in neurodegenerative diseases: a potential role for membrane fluidity disturbance. *Br. J. Pharmacol.* 163:1379–1390.
26. Spillantini, M. G., M. L. Schmidt, …, M. Goedert. 1997. Alpha-synuclein in Lewy bodies. *Nature.* 388:839–840.
27. Levitan, K., D. Chereau, …, G. L. Millhauser. 2011. Conserved C-terminal charge exerts a profound influence on the aggregation rate of α-synuclein. *J. Mol. Biol.* 411:329–333.
28. Buell, A. K., C. Galvagnion, …, C. M. Dobson. 2014. Solution conditions determine the relative importance of nucleation and growth processes in α-synuclein aggregation. *Proc. Natl. Acad. Sci. USA.* 111:7671–7676.
29. Reynolds, N. P., A. Soragni, …, S. Seeger. 2011. Mechanism of membrane interaction and disruption by α-synuclein. *J. Am. Chem. Soc.* 133:19366–19375.
30. van Maarschalkerweerd, A., V. Vetri, …, B. Vestergaard. 2014. Protein/lipid coaggregates are formed during α-synuclein-induced disruption of lipid bilayers. *Biomacromolecules.* 15:3643–3654.

31. Andreasen, M., N. Lorenzen, and D. Otzen. 2015. Interactions between misfolded protein oligomers and membranes: a central topic in neurodegenerative diseases? *Biochim. Biophys. Acta.* 1848:1897–1907.
32. Bussell, R., Jr., T. F. Ramlall, and D. Eliezer. 2005. Helix periodicity, topology, and dynamics of membrane-associated α-synuclein. *Protein Sci.* 14:862–872.
33. Burke, K. A., E. A. Yates, and J. Legleiter. 2013. Biophysical insights into how surfaces, including lipid membranes, modulate protein aggregation related to neurodegeneration. *Front. Neurol.* 4:17.
34. Dikiy, I., and D. Eliezer. 2012. Folding and misfolding of alpha-synuclein on membranes. *Biochim. Biophys. Acta.* 1818:1013–1018.
35. Iyer, A., N. O. Petersen, …, V. Subramaniam. 2014. Amyloids of alpha-synuclein affect the structure and dynamics of supported lipid bilayers. *Biophys. J.* 106:2585–2594.
36. Giasson, B. I., I. V. Murray, …, V. M. Lee. 2001. A hydrophobic stretch of 12 amino acid residues in the middle of alpha-synuclein is essential for filament assembly. *J. Biol. Chem.* 276:2380–2386.
37. Hoyer, W., D. Cherny, …, T. M. Jovin. 2004. Impact of the acidic C-terminal region comprising amino acids 109–140 on alpha-synuclein aggregation in vitro. *Biochemistry.* 43:16233–16242.
38. van Raaij, M. E., I. M. Segers-Nolten, and V. Subramaniam. 2006. Quantitative morphological analysis reveals ultrastructural diversity of amyloid fibrils from alpha-synuclein mutants. *Biophys. J.* 91:L96–L98.
39. Rhoades, E., T. F. Ramlall, …, D. Eliezer. 2006. Quantification of alpha-synuclein binding to lipid vesicles using fluorescence correlation spectroscopy. *Biophys. J.* 90:4692–4700.
40. Schindelin, J., I. Arganda-Carreras, …, A. Cardona. 2012. Fiji: an open-source platform for biological-image analysis. *Nat. Methods.* 9:676–682.
41. Soumpasis, D. M. 1983. Theoretical analysis of fluorescence photobleaching recovery experiments. *Biophys. J.* 41:95–97.
42. Seu, K. J., L. R. Cambrea, …, J. S. Hovis. 2006. Influence of lipid chemistry on membrane fluidity: tail and headgroup interactions. *Biophys. J.* 91:3727–3735.
43. Ramakrishnan, M., P. H. Jensen, and D. Marsh. 2003. Alpha-synuclein association with phosphatidylglycerol probed by lipid spin labels. *Biochemistry.* 42:12919–12926.
44. Naiki, H., K. Higuchi, …, T. Takeda. 1989. Fluorometric determination of amyloid fibrils in vitro using the fluorescent dye, thioflavin T1. *Anal. Biochem.* 177:244–249.
45. LeVine, H., 3rd 1999. Quantification of beta-sheet amyloid fibril structures with thioflavin T. *Methods Enzymol.* 309:274–284.
46. Galvagnion, C., A. K. Buell, …, C. M. Dobson. 2015. Lipid vesicles trigger α-synuclein aggregation by stimulating primary nucleation. *Nat. Chem. Biol.* 11:229–234.
47. Lindblom, G., and G. Orädd. 2009. Lipid lateral diffusion and membrane heterogeneity. *Biochim. Biophys. Acta.* 1788:234–244.
48. Mulders, F., H. van Langen, …, Y. K. Levine. 1986. The static and dynamic behaviour of fluorescent probe molecules in lipid bilayers. *Biochim. Biophys. Acta.* 859:209–218.
49. Lentz, B. R. 1993. Use of fluorescent probes to monitor molecular order and motions within liposome bilayers. *Chem. Phys. Lipids.* 64:99–116.
50. Vats, K., K. Knutson, …, E. D. Sheets. 2010. Peripheral protein organization and its influence on lipid diffusion in biomimetic membranes. *ACS Chem. Biol.* 5:393–403.
51. Leftin, A., C. Job, …, M. F. Brown. 2013. Solid-state ^{13}C NMR reveals annealing of raft-like membranes containing cholesterol by the intrinsically disordered protein α-synuclein. *J. Mol. Biol.* 425:2973–2987.
52. Bagatolli, L. A., J. H. Ipsen, …, O. G. Mouritsen. 2010. An outlook on organization of lipids in membranes: searching for a realistic connection with the organization of biological membranes. *Prog. Lipid Res.* 49:378–389.
53. Jensen, M. O., and O. G. Mouritsen. 2004. Lipids do influence protein function-the hydrophobic matching hypothesis revisited. *Biochim. Biophys. Acta.* 1666:205–226.
54. Weaver, T. E., and J. J. Conkright. 2001. Function of surfactant proteins B and C. *Annu. Rev. Physiol.* 63:555–578.
55. Fortin, D. L., M. D. Troyer, …, R. H. Edwards. 2004. Lipid rafts mediate the synaptic localization of alpha-synuclein. *J. Neurosci.* 24:6715–6723.
56. Middleton, E. R., and E. Rhoades. 2010. Effects of curvature and composition on α-synuclein binding to lipid vesicles. *Biophys. J.* 99:2279–2288.
57. Cole, N. B., D. D. Murphy, …, R. L. Nussbaum. 2002. Lipid droplet binding and oligomerization properties of the Parkinson's disease protein alpha-synuclein. *J. Biol. Chem.* 277:6344–6352.
58. Levi, M., P. Wilson, …, T. Parasassi. 1997. In K562 and HL60 cells membrane ageing during cell growth is associated with changes in cholesterol concentration. *Mech. Ageing Dev.* 97:109–119.
59. Scholtz, J. M., H. Qian, …, R. L. Baldwin. 1991. Parameters of helix-coil transition theory for alanine-based peptides of varying chain lengths in water. *Biopolymers.* 31:1463–1470.

Biophysical Journal, Volume *111*

Supplemental Information

Membrane-Bound Alpha Synuclein Clusters Induce Impaired Lipid Diffusion and Increased Lipid Packing

Aditya Iyer, Nathalie Schilderink, Mireille M.A. E. Claessens, and Vinod Subramaniam

Supporting Information

Membrane-Bound Alpha Synuclein Clusters Induce Impaired Lipid Diffusion and Increased Lipid Packing

[†‡1]Aditya Iyer, [‡]Nathalie Schilderink, [‡]Mireille M.A.E Claessens and [†‡‖]Vinod Subramaniam

[†]Nanoscale Biophysics Group, FOM Institute AMOLF, Amsterdam, The Netherlands

[‡]Nanobiophysics Group, MESA+ Institute for Nanotechnology, University of Twente, Enschede, The Netherlands

[‖]Vrije Universiteit Amsterdam, De Boelelaan 1105, 1081 HV Amsterdam, The Netherlands

[1] Aditya Iyer's present address is Membrane Enzymology Group, Groningen Institute of Biomolecular Sciences & Biotechnology, University of Groningen, Groningen, The Netherlands

Table of Contents

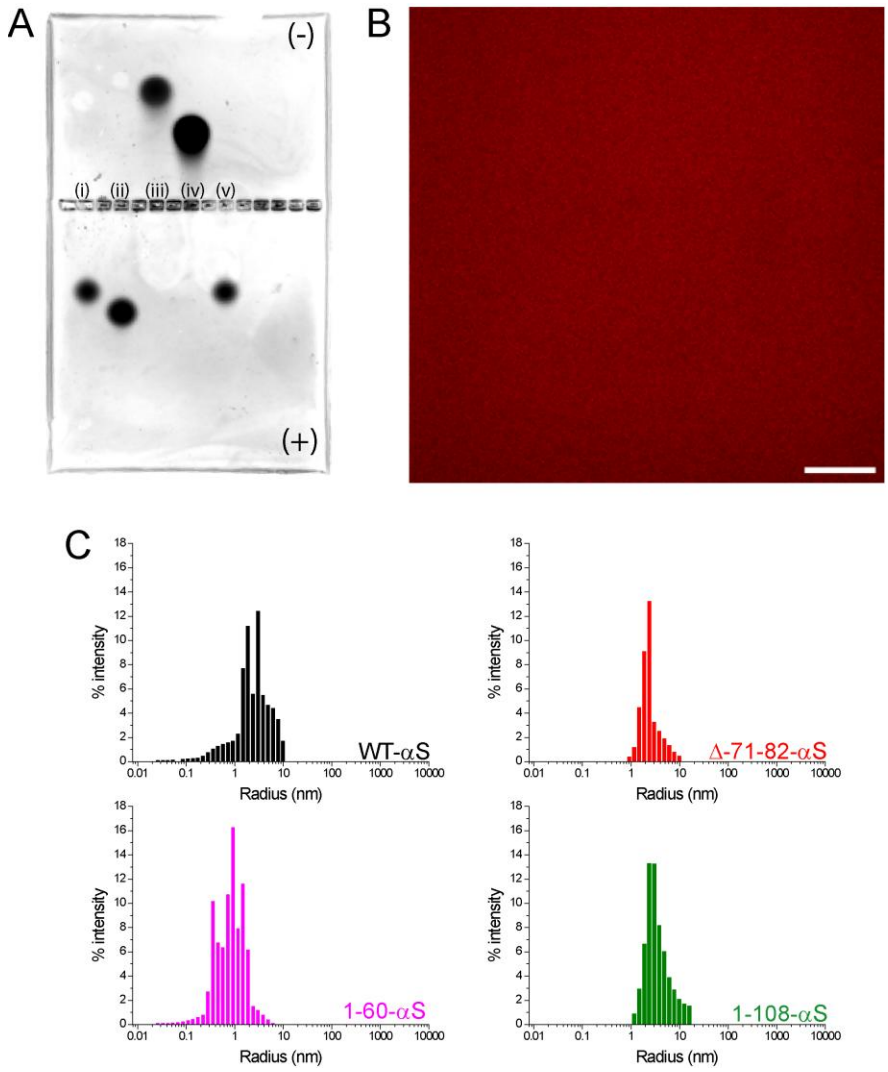

Fig S1: Characterization of monomeric state of αS and effect of bare glass. A) Non-denaturing agarose gel for WT-αS (lane i and v) and deletion variants. 10 µM of αS samples were aliquoted into wells in a 0.5% Agarose gel in Tris-Glycine buffer at pH 8. Since 1-60-αS (lane iii) and 1-108-αS (lane iv) deletion variants have a net positive charge at pH 7.4, an agarose gel was run with wells in middle to allow migration to both charged poles. The Δ71-82-αS deletion variant is shown in lane ii. B) Fluorescence image of 10 µM monomeric WT-αS (10% labeled AlexaFluor647 labeled WT-αS) on bare glass surface. Images were acquired within 1 minute of αS incubation on the glass slide. The scale bar is 10 µm. All experiments were performed in 50 mM HEPES, 0.1 mM EDTA, pH 7.4 buffer at room temperature. C) Distributions of hydrodynamic radii of WT-αS and αS deletion variants obtained by dynamic light scattering confirming absence of higher ordered species.

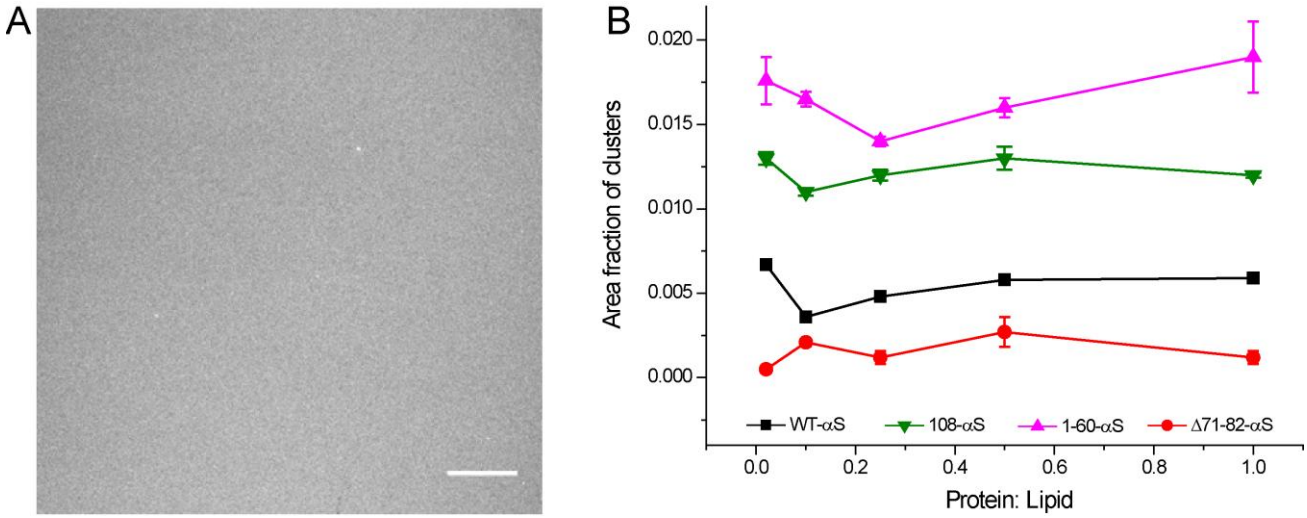

Fig S2: A) Fluorescence image of SLBs obtained before addition of αS. B) Overview of area fractions of αS clusters on POPC:POPG SLBs. The above plot depicts area fraction of αS clusters obtained from fluorescent images after image processing (see methods) starting from a protein:lipid ratio of 0.02.

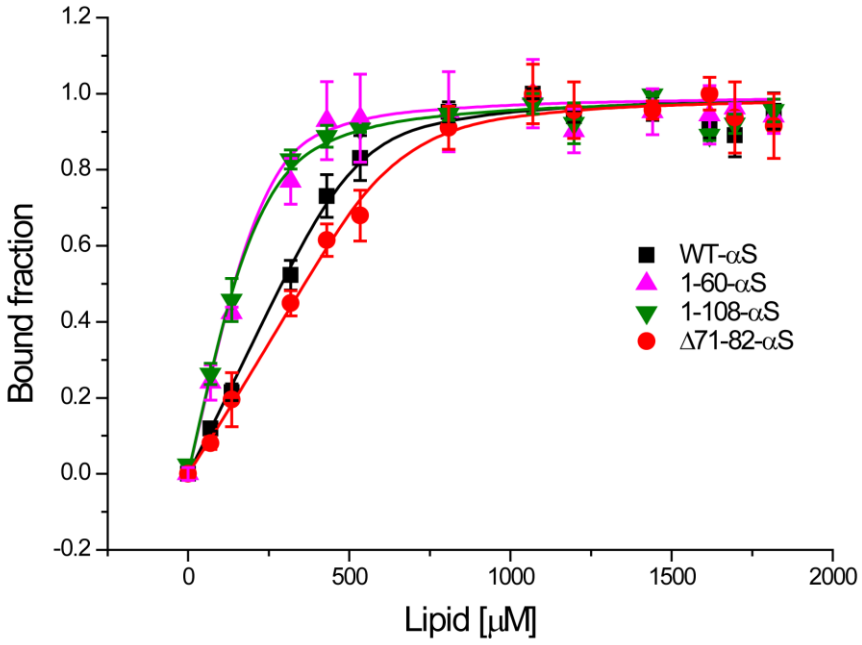

αS type	Aggregation into amyloids	Net charge at pH 7.4	Mean residue ellipticity (mdeg.cm^2.dmol^{-1})	% α-helical content,H	Size of helix, amino acids	Lipid concentration at 50% αS binding
Δ71-82-αS	-	-9.9	13077 ± 587	36 ± 2	47 ± 3	359 ± 24
WT-αS	+	-8.9	20758 ± 687	56 ± 3	79 ± 4	293 ± 24
1-60-αS	-	+4.1	18306 ± 971	51 ± 3	31 ± 5	155 ± 10
1-108-αS	+++	+3.1	26684 ± 914	73 ± 3	79 ± 4	144 ± 17

Fig S3: Binding of WT-αS and other truncated variants to POPC:POPG liposomes. The bound fractions were obtained by measuring mean residual ellipticites at 222 nm by CD spectroscopy. The binding curve was quantified by fitting normalized mean residual ellipticity values. The error bars indicate standard deviations from three independent measurements. All experiments were carried out in 50 mM HEPES, 0.1 mM EDTA, pH 7.4 buffer at room temperature. The calculation of helicity was performed as described elsewhere (1). Briefly, $\mathbf{H = 100 * (\theta - \theta_{coil})/(\theta_{\alpha} - \theta_{coil})}$ where H is % helicity, $\boldsymbol{\theta}$ is the measured mean-residual ellipticity at 222 nm, $\boldsymbol{\theta_{\alpha}}$ and $\boldsymbol{\theta_{coil}}$ are the mean residual ellipticites at 222 nm of idealized α-helical and random coil peptides, respectively, calculated as follows: $\boldsymbol{\theta_{\alpha} = -40000 * \left(1 - \frac{2.5}{n}\right) + 100 * t}$; $\boldsymbol{\theta_{coil} = 640 - 45 * t}$ where t is temperature in Celsius and n is the number of amino acids in the peptide. From the values of H, the approximate numbers of residues forming a helix were calculated.

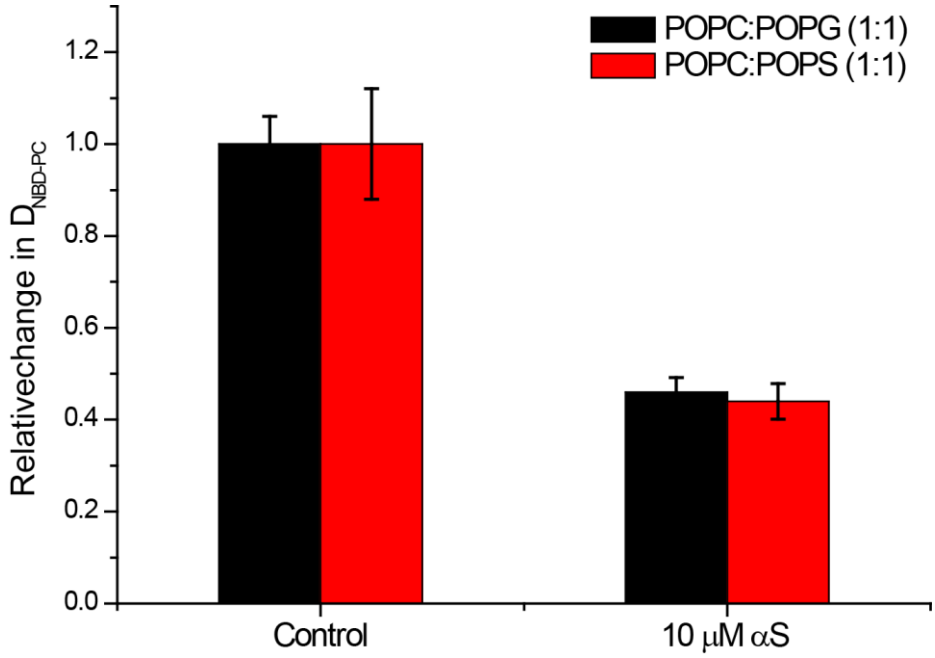

Fig S4: Influence of WT-αS on the D_{NBD-PC} in SLBs with different lipid headgroups. 10 μM of WT-αS was incubated on SLBs composed of equimolar ratios of POPC:POPG (black bars) and POPC:POPS (red bars). The D_{NBD-PC} values were normalized with respect to that obtained in absence of any added protein. All experiments were performed in 50 mM HEPES, 0.1 mM EDTA, pH 7.4 buffer at room temperature.

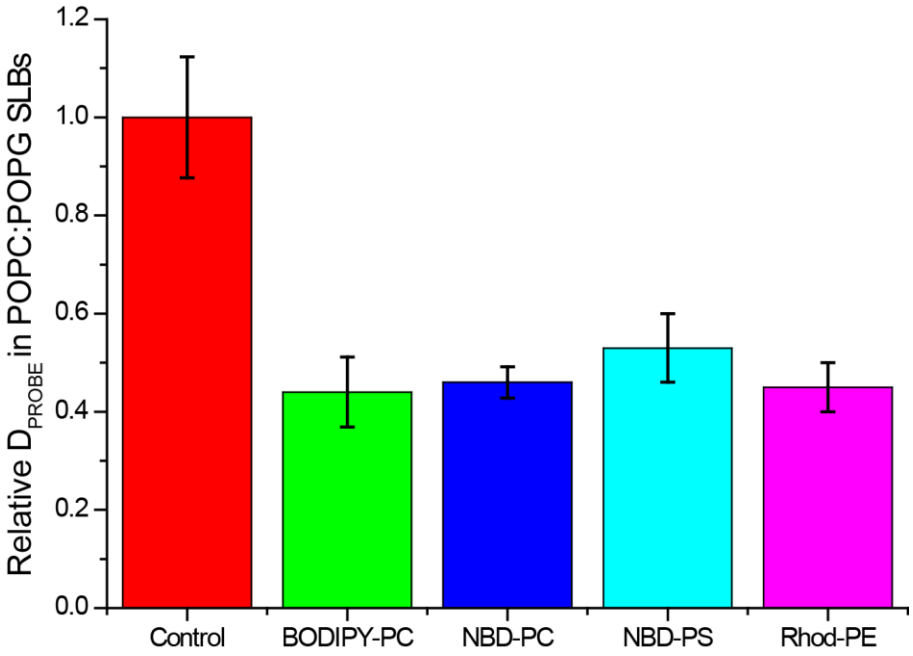

Fig S5: Relative change in the D_{LL} of different probes in POPC:POPG SLBs. POPC:POPG (1:1) SLBs were prepared in 50 mM HEPES, 0.1 mM EDTA, pH 7.4 buffer at room temperature. The fluorescent lipid probe concentration was 0.5 mol% in each case. 10 μM of WT-αS was incubated with POPC:POPG SLBs and D_{PROBE} was measured immediately. NBD-PC and BODIPY-PC have a zwitterionic PC headgroup and the fluorophore is covalently linked in the acyl chain. The Rhod-PE probe is headgroup labeled and negatively charged while the NBD-PS probe is acyl chain labeled and negatively charged. The similar magnitude of change in the D_{PROBE} suggests that the type of fluorescent lipid probe does not influence our observations.

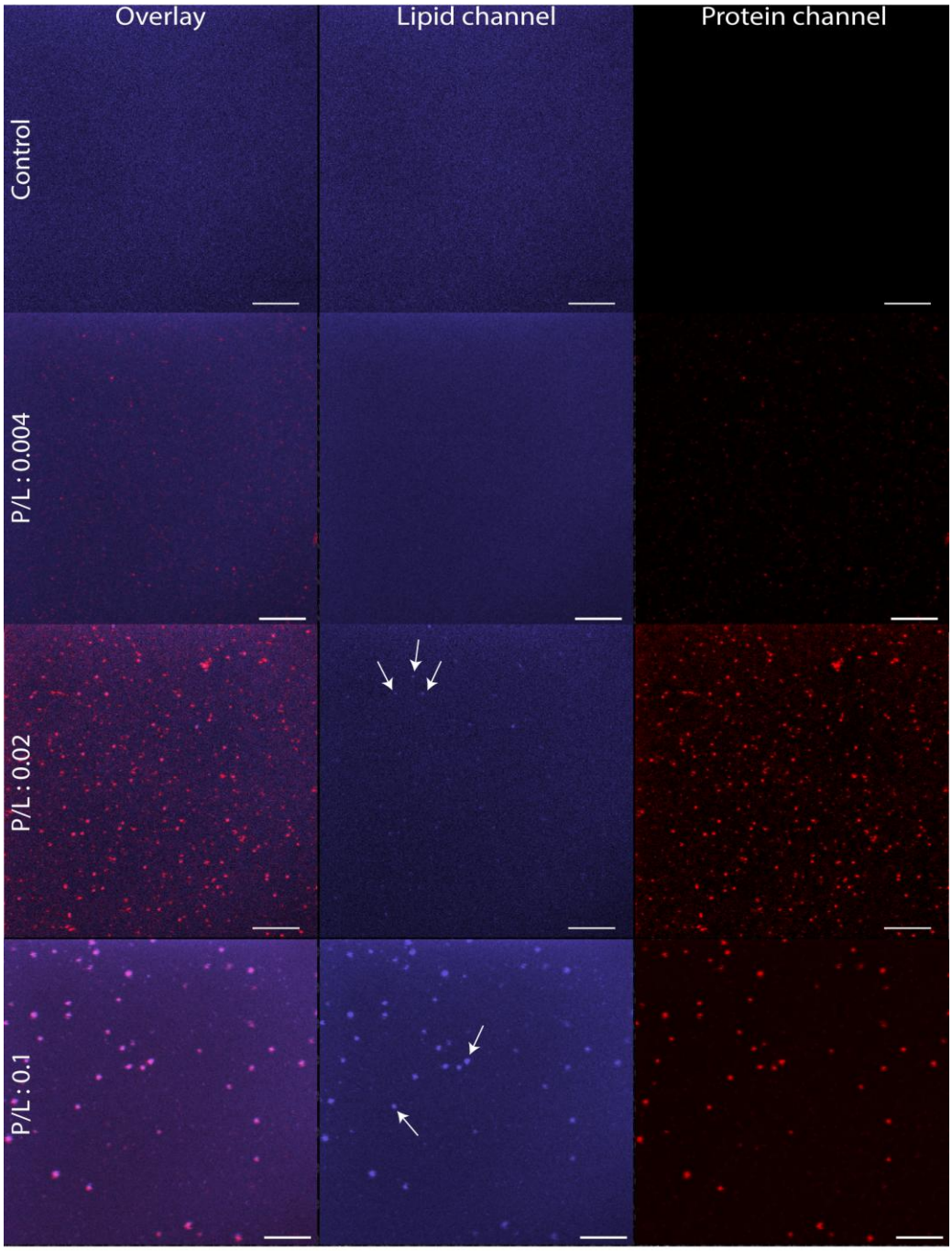

Fig S6: WT-αS induced lipid ordering in POPC:POPG SLBs observed using DPH. Incubation of increasing concentrations of monomeric αS, or increased P/L ratios a shown in figure above resulted in intense fluorescent regions (white arrows in lipid channel) upon larger cluster formation (protein channel). POPC:POPG SLBs were labeled with 1 mol% DPH. All experiments were carried out in 50 mM HEPES buffer, 0.1 mM EDTA, pH 7.4 at room temperature. The scale bar is 10 µm.

Supporting References

1. Scholtz, J. M., H. Qian, E. J. York, J. M. Stewart, and R. L. Baldwin. 1991. Parameters of Helix-Coil Transition Theory for Alanine-Based Peptides of Varying Chain Lengths in Water. Biopolymers 31:1463-1470.